

Reaction Sequence and Electrochemical Properties of Lithium Nickel Manganese Oxide Cathode Materials Synthesized Via Hydrothermal Reaction Followed by Subsequent Heat Treatment

Ji Eun Park, Kyungho Kim, Su Han Park, Eun Su Park, Mu Wook Pyeon and Man-Jong Lee*

Department of Advanced Technology Fusion, Konkuk University, 1 Hwayang-dong, Kwangjin-gu, Seoul 143-701, Republic of Korea

*E-mail: leemtx@konkuk.ac.kr

Received: 25 February 2013 / Accepted: 28 March 2013 / Published: 1 May 2013

Lithium nickel manganese oxide ($\text{LiNi}_{0.5}\text{Mn}_{1.5}\text{O}_4$) cathode materials were synthesized via a hydrothermal reaction followed by heat treatment at 600, 700, and 800 °C. From both X-ray diffraction (XRD) and thermogravimetry/differential thermal analysis (TG/DTA), a detailed reaction sequence for the formation of $\text{LiNi}_{0.5}\text{Mn}_{1.5}\text{O}_4$ is proposed. By comparing the materials synthesized with and without the hydrothermal reaction, the effectiveness of the hydrothermal treatment on the final electrochemical properties was evaluated. $\text{LiNi}_{0.5}\text{Mn}_{1.5}\text{O}_4$ cathodes with different thermal-treatment histories showed clear differences in morphology, size, and crystallinity. Samples that were subsequently heat-treated at 600 and 700 °C showed a highly agglomerated morphology. In contrast, the sample heat treated at 800 °C resulted in octahedral particles with increased particle size, increased crystallinity, and decreased agglomeration. Such differences clearly influenced the electrochemical properties of the materials. $\text{LiNi}_{0.5}\text{Mn}_{1.5}\text{O}_4$ cathode materials heat-treated at 600, 700, and 800 °C showed initial discharge capacities of 94.60, 113.88, and 131.78 mAh/g, respectively, and discharge capacities of 80.24, 93.61, and 123.36 mAh/g, respectively, after 40 cycles. The improved cyclability of the $\text{LiNi}_{0.5}\text{Mn}_{1.5}\text{O}_4$ cathode material that was heat-treated at 800 °C is due to its increased crystallinity and structural stability.

Keywords: $\text{LiNi}_{0.5}\text{Mn}_{1.5}\text{O}_4$, battery cathode, reaction sequence, hydrothermal reaction, crystallinity.

1. INTRODUCTION

Spinel lithium manganese oxide (LiMn_2O_4) has been extensively researched for use as a cathode material in rechargeable lithium batteries owing to its low cost, environmental friendliness,

and the abundance of manganese resources [1]. It is also regarded as one of the most viable candidates for high-power cathode materials due to its structural stability [2]. However, practical applications of LiMn_2O_4 cathodes face some problems: (i) Jahn–Teller distortion due to the phase transition from a cubic to a tetragonal phase [3], (ii) dissolution of Mn ions at high electrode potentials in the presence of acid impurities originating from $\text{Mn}^{3+/4+}$ redox reaction [4], (iii) instability of electrolyte at high voltages, and (iv) formation of oxygen vacancies because of the dissolution of manganese in the electrolyte [5,6]. These phenomena result in capacity decay and poor cycling stability. As an effective approach to improving the poor cycling behavior of LiMn_2O_4 , the use of metal-substituted spinel materials ($\text{LiM}_x\text{Mn}_{2-x}\text{O}_4$, M = Cr, Co, Fe, Cu, Al, etc.) has been suggested [7]. These cathode materials generally show two separate voltage plateaus at approximately 4.0 and 5.0 V [7–10]. In contrast, nickel-substituted spinel ($\text{LiNi}_{0.5}\text{Mn}_{1.5}\text{O}_4$) shows two dominant plateaus at approximately 4.7 V, significantly improving the cycling performance [9]. The characteristic potential plateaus of $\text{LiNi}_{0.5}\text{Mn}_{1.5}\text{O}_4$ at ~4.7 V are attributed to two redox reactions between $\text{Ni}^{2+}/\text{Ni}^{3+}$ and $\text{Ni}^{3+}/\text{Ni}^{4+}$, which result in a high discharge capacity with quite stable cyclic retention owing to fast electron-transfer kinetics [7–10].

It is well known that the electrochemical properties of $\text{LiNi}_{0.5}\text{Mn}_{1.5}\text{O}_4$ materials are highly dependent on the preparation conditions [11], crystallinity [12], oxidation state of Mn ions [13], and morphology changes [14]. Generally, solid-state synthesis requires a large amount of thermal energy (>800 °C) and long reaction times (>24 h). Furthermore, accurate control of Li:Ni:Mn ratio is difficult due to the evaporation of Li sources [15]. A variety of techniques have been developed to overcome the drawbacks of conventional solid-state synthesis of $\text{LiNi}_{0.5}\text{Mn}_{1.5}\text{O}_4$. These include a sol-gel process [8,16], coprecipitation [11], emulsion drying [15], a composite carbonate process [17], molten salt [18], combustion [19], an ultrasonic spray pyrolysis method [20], and a hydrothermal reaction [21]. Although the hydrothermal method is attractive to industry owing to the facile and cost-effective formation of advanced materials, there are only a few reports on the synthesis of $\text{LiNi}_{0.5}\text{Mn}_{1.5}\text{O}_4$ using this technique.

In this study, we synthesized $\text{LiNi}_{0.5}\text{Mn}_{1.5}\text{O}_4$ cathode materials using the hydrothermal technique followed by a subsequent heat treatment and evaluated the effectiveness of the two-step process in the formation of high-quality $\text{LiNi}_{0.5}\text{Mn}_{1.5}\text{O}_4$ cathode materials. Because $\text{LiNi}_{0.5}\text{Mn}_{1.5}\text{O}_4$ materials undergo a complex reaction throughout the process, the exact reaction sequence for the formation of $\text{LiNi}_{0.5}\text{Mn}_{1.5}\text{O}_4$ is elucidated by considering each step during the hydrothermal reaction and subsequent heat treatment, which has not been reported before. Furthermore, the effect of different thermal histories on the morphology and electrochemical properties of $\text{LiNi}_{0.5}\text{Mn}_{1.5}\text{O}_4$ is discussed.

2. EXPERIMENTAL

2.1. Material synthesis and characterization

Pure LiOH (>99%, Sigma-Aldrich), $\text{Ni}(\text{NO}_3)_2 \cdot 6\text{H}_2\text{O}$ (>99%, Sigma-Aldrich), and $\text{Mn}(\text{NO}_3)_2 \cdot 4\text{H}_2\text{O}$ (>99%, Alfa Aesar) were used as raw materials without any purification. First,

stoichiometric LiOH, Ni(NO₃)₂·6H₂O, and Mn(NO₃)₂·4H₂O (Li:Ni:Mn = 1:0.5:1.5) were added to distilled water under magnetic stirring at room temperature. After 1 h, all the precursors completely dissolved in the distilled water and the reaction solution changed from brown to black. The solution was then transferred to a Teflon-lined stainless-steel autoclave (120-mL capacity). The mixture was subjected to hydrothermal conditions at 200 °C for 12 h. After the hydrothermal reaction, the solution was dried at 100 °C in air until a black powder was formed. The powders were heat-treated at 600, 700, and 800 °C for 12 h followed by passive cooling to room temperature to form LiNi_{0.5}Mn_{1.5}O₄ cathode materials, which are denoted hereafter as LNM600, LNM700, and LNM800. For comparison, LiNi_{0.5}Mn_{1.5}O₄ cathode materials were also synthesized at 800 °C for 12 h following the same procedures but without the hydrothermal treatment; this control sample is denoted as LNM800wt.

The crystal structures of the as-prepared and heated powders were determined using X-ray diffraction (XRD, X'Pert pro MPD, PANalytica, generator 45 kW) with Cu K α radiation. The morphologies and particle sizes of the samples were analyzed via field emission scanning electron microscopy (FE-SEM, Hitachi SU-70, resolution: >1.0 nm at 15 kV acceleration). Thermogravimetry/differential thermal analysis (TG/DTA) was performed using a thermal analysis system (TG/DTA, SDT Q600).

2.2. Electrochemical measurements

The working electrode was prepared by pressing a mixture of the active cathode material, conductive material (Super P[®] carbon black), and binder (polyvinylidene fluoride, PVDF) at ratio 80:15:5 (w/w). The mixtures were dissolved in 1-methyl-2-pyrrolidinone (NMP) to form slurries and then uniformly cast on thick aluminum foil (thickness 0.01 mm, 99.9% trace metal basis). Li foil was used as the reference electrode. The electrolyte (Solvent Company, Korea) was 1 M LiPF₆ dissolved in a 1:1 (volume) mixture of ethylene carbonate (EC) and diethyl carbonate (DEC). The test cells (CR2016 coin-type) were assembled under a high-purity argon atmosphere in a glove box (M. O. Tech, Korea) using a separator (polypropylene 2600). The discharge/charge tests were performed at room temperature using an automatic battery tester system (WBCS 3000, Wonatech, Korea). Discharge/charge measurements were performed in the range 3.5–5.0 V at various current densities (1 C).

3. RESULTS AND DISCUSSION

3.1. Reaction sequence of lithium nickel manganese oxide

The first step in the sample preparation involves the dissolution of the LiOH, Ni(NO₃)₂·6H₂O, and Mn(NO₃)₂·4H₂O precursors in distilled water at room temperature. The reaction mixture was then hydrothermally reacted at 200 °C for 12 h and dried at 100 °C to form powders, which were analyzed by XRD (Fig. 1). After the hydrothermal reaction, the samples showed mixed crystal phases, including

single-phase $\text{LiNi}_{0.5}\text{Mn}_{1.5}\text{O}_4$ and intermediate phases LiMn_2O_4 and NiMnO_3 . On analyzing the XRD studies, the following reactions can be suggested as occurring during the hydrothermal reaction:

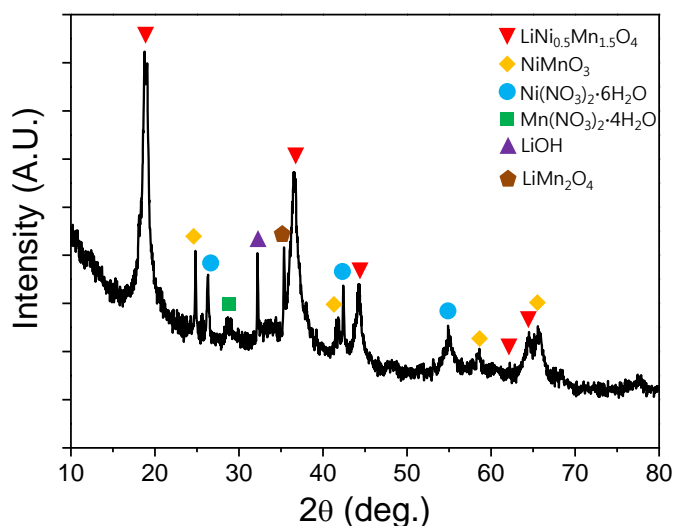
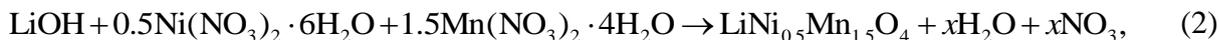
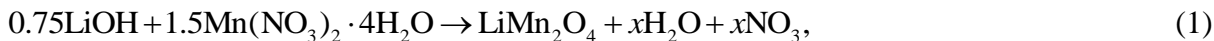


Figure 1. XRD patterns after the hydrothermal reaction.

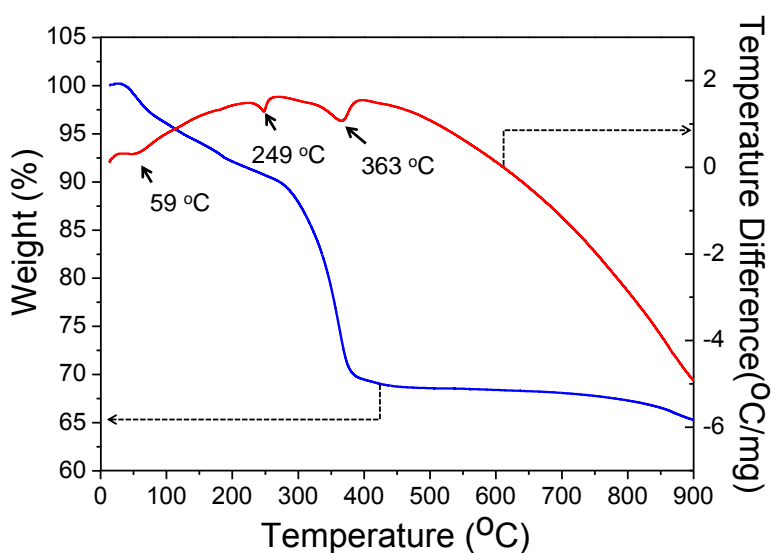


Figure 2. TG/DTA results of samples up to 900 °C.

It should be noted that the intermediate compounds LiMn_2O_4 and NiMnO_3 easily react to form $\text{LiNi}_{0.5}\text{Mn}_{1.5}\text{O}_4$ in the presence of lithium ions [22,23]. These intermediate compounds thus can play an important role in the crystallization and morphology evolution during the subsequent heat-treatment procedure.

To determine the ideal heat-treatment temperature in the formation of $\text{LiNi}_{0.5}\text{Mn}_{1.5}\text{O}_4$, TG/DTA measurements were performed and the results are shown in Fig. 2. Based on TG/DTA, the thermal decomposition of the precursors can be divided into several stages: first, from room temperature to 140 °C, wherein a weight loss of ~7 wt% was detected with an endothermic peak on the DTA curve, which could be attributed to the loss of water from the precursors. Above 140 °C, the weight loss rapidly increased with increase in temperature. Considerable weight loss (~5%) was observed in the second stage in the range 140–250 °C, which indicates active combustion and decomposition of the precursors. At this stage, endothermic peaks were found at 249 °C, as shown in Fig. 2, which correspond to the evaporation of residual nitrate phases. In the last stage, in the range 250–400 °C, additional weight loss (~18%) was observed, which could be considered the result of melting of LiOH and the formation of $\text{LiNi}_{0.5}\text{Mn}_{1.5}\text{O}_4$ by the complete decomposition of the nitrates. Above 400 °C, no other thermal phenomena could be found [24].

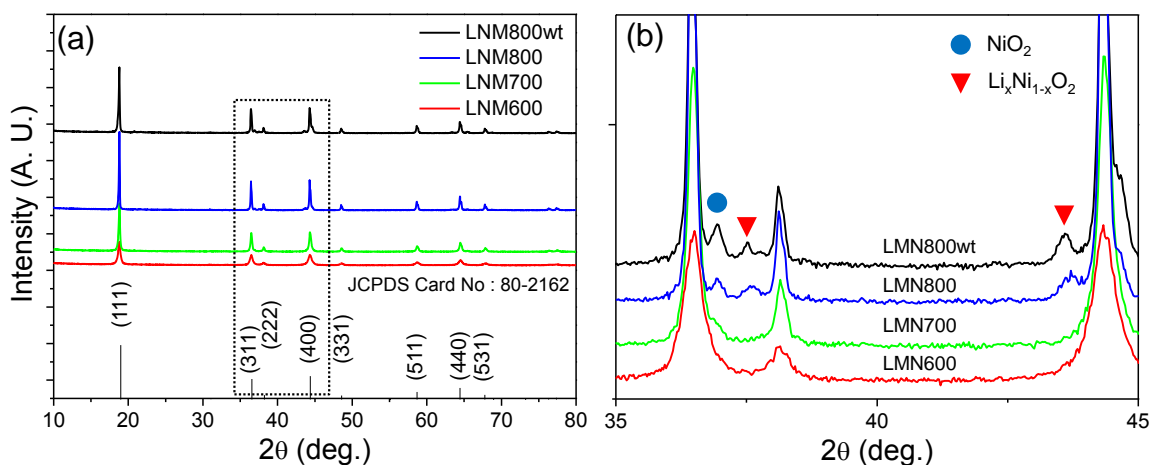
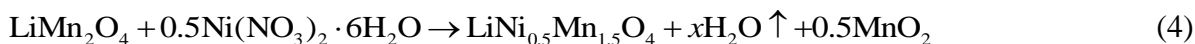


Figure 3. (a) XRD pattern of $\text{LiNi}_{0.5}\text{Mn}_{1.5}\text{O}_4$ by the different heat-treatment temperatures, and (b) enlarged area of hatched box in (a).

To synthesize single-phase $\text{LiNi}_{0.5}\text{Mn}_{1.5}\text{O}_4$, the dried black powders were heat treated at 600, 700, and 800 °C, and the resulting XRD patterns are shown in Fig. 3. Considering the increase of the (111) peak at 18.8° with increase in the heat-treatment temperature, it is evident that higher temperatures increase the crystallinity of the $\text{LiNi}_{0.5}\text{Mn}_{1.5}\text{O}_4$ phase (JCPDS Card No.:80-2162) [16]. From the XRD analyses at various heat-treatment temperatures (Figs. 3a and b), an accurate reaction sequence for the formation of single-phase $\text{LiNi}_{0.5}\text{Mn}_{1.5}\text{O}_4$ (600, 700 °C) can be suggested as follows [22,23]:





Above 800 °C, impurities such as NiO₂ and Li_xNi_{1-x}O were detected (Fig. 3b). According to Bruce et al. [25], such impurities form at high temperature because of the change in the oxidation state of Mn. The TG/DTA studies provide evidences shown in Eqs. 4–6 including the evaporation of residual H₂O as well as the chemically bound H₂O and NO₃ in the precursors. The overall reaction sequence during the hydrothermal treatment and subsequent heat treatment is summarized in Table 1.

Table 1. Overall reaction sequence for the formation of LiNi_{0.5}Mn_{1.5}O₄.

| | LiOH | Ni(NO ₃) ₂ ·6H ₂ O | Mn(NO ₃) ₂ ·4H ₂ O | NiMnO ₃ | LiMn ₂ O ₄ | LiNi _{0.5} Mn _{1.5} O ₄ | NiO ₂ | Li _x Ni _{1-x} O |
|------------------------------------|------|--|--|--------------------|----------------------------------|--|------------------|-------------------------------------|
| Precursors dissolution | O | O | O | X | X | X | X | X |
| Hydrothermal reaction ^a | ↓ | ↓ | ↓ | O | O | O | X | X |
| Heating (600 °C) | X | X | X | X | X | ↑ | X | X |
| Heating (700 °C) | X | X | X | X | X | ↑ | X | O |
| Heating (800 °C) | X | X | X | X | X | ↑ | O | → |

^a 200 °C for 12 h; O first formed; ↓ amount decreased; ↑ amount increased; → amount constant

Note that the hydrothermal treatment significantly enhanced the crystallinity after the subsequent heat treatment, despite the comparatively lower degree of crystallinity of the control LNM800wt material shown in Fig. 3a. Thus, we can conclude from the reaction-sequence study that the presence of small-sized LiNi_{0.5}Mn_{1.5}O₄ phase and the intermediate LiMn₂O₄ and NiMnO₃ phases formed by the prior hydrothermal process boosted the formation and crystallinity of the LiNi_{0.5}Mn_{1.5}O₄ phase.

3.2. Morphology of lithium nickel manganese oxide

Figure 4 shows the SEM images of LNM600 (Fig. 4a), LNM700 (Fig. 4b), and LNM800 (Fig. 4c). Figure 4d shows the image of the control sample LNM800wt for comparison. The morphology and size of the as-synthesized LiNi_{0.5}Mn_{1.5}O₄ compound is significantly influenced by the heat-treatment temperature, which is similar to previous reports [8,15,16]. Both LNM600 and LNM700 are highly agglomerated compared to LNM800. Interestingly, the as-synthesized LNM800 contains octahedral particles with diameters in the range 300–500 nm. In contrast, the as-synthesized LNM600 shows highly agglomerated and irregularly shaped nanoparticles with diameters in the range 80–100 nm. In the case of LNM700, the particle size gradually increased up to 150–250 nm with a decrease in particle irregularity. On comparing LNM800 (with hydrothermal process) and LNM800wt (without hydrothermal process), we found that LNM800 shows a much smaller particle size and more

homogeneously distributed particle characteristics, demonstrating the effectiveness of the hydrothermal treatment before the heat treatment.

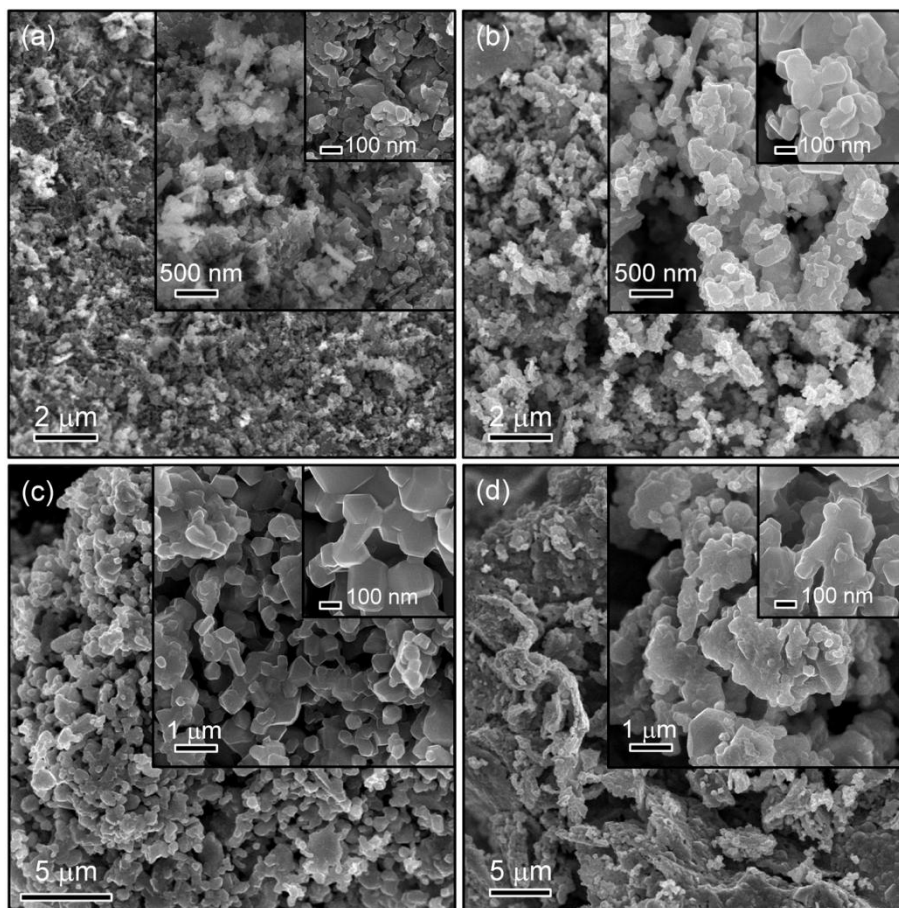


Figure 4. SEM images of spinel $\text{LiNi}_{0.5}\text{Mn}_{1.5}\text{O}_4$ synthesized by the heat treatment at 600 (a), 700 (b), and 800 °C (c) after the hydrothermal reaction, and for comparison the SEM image of $\text{LiNi}_{0.5}\text{Mn}_{1.5}\text{O}_4$ synthesized by the heat treatment at 800 °C (d) without hydrothermal reaction. SEM images of LNM600 (a), LNM700 (b), LNM800 (c), and LNM800wt (d).

Although it is not shown here, cathode materials fabricated without prior hydrothermal processing do not show homogeneously distributed particle characteristics in the heat-treatment temperature range 600–900 °C.

3.3. Electrochemical performance of lithium nickel manganese oxide

To determine the effect of different heat-treatment temperatures on the electrochemical behavior of $\text{LiNi}_{0.5}\text{Mn}_{1.5}\text{O}_4$ during Li^+ insertion/extraction, the charge/discharge behavior and differential capacity (dQ/dV) characteristics of the $\text{LiNi}_{0.5}\text{Mn}_{1.5}\text{O}_4$ cathode materials were measured at current density 1 C (147 mAh/g) at room temperature between 3.5 and 5.0 V (vs. Li/Li^+). Figure 5a shows the initial capacities while Fig. 5b shows the differential capacities of LNM600, LNM700, and

LNM800. LNM800 showed a higher initial capacity (Fig. 5a), and the reduction/oxidation peaks of the first cycle were significantly distinct compared to those of LNM600 and LNM700 (Fig. 5b).

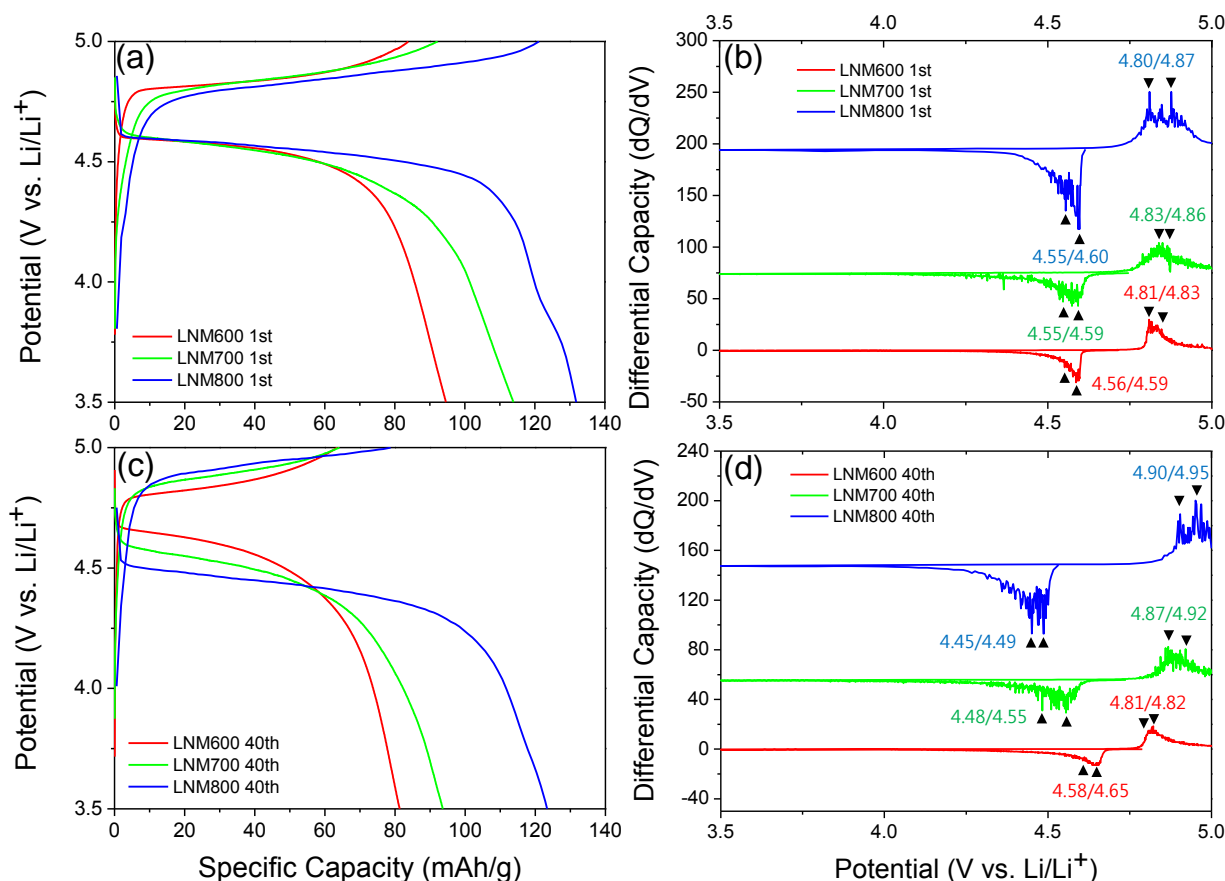


Figure 5. Charge–discharge behaviors at the first (a) and 40th (c) cycles, and differential capacity (dQ/dV) at the first (b) and 40th (d) cycles of the $\text{LiNi}_{0.5}\text{Mn}_{1.5}\text{O}_4$ cathode materials measured at 1 C and room temperature with a potential range between 3.5 and 5.0 V (vs. Li/Li^+).

The initial discharge capacities of LNM600, LNM700, and LNM800 were 94.65, 113.88, and 131.78 mAh/g, respectively. By a simple hydrothermal reaction followed by heat treatment at 800 °C, we found that LNM800 shows an improved initial capacity compared to that found in other reports [8,16,11,15,25], which suggests that the present synthesis process is effective. Although impurities such as NiO_2 and $\text{Li}_x\text{Ni}_{1-x}\text{O}$ were detected, LNM800 showed better electrochemical properties, which may be because of the increased structural stability resulting from the distribution of oxidized Mn^{3+} ions [16]. Li^+ insertion/extraction during the first charge/discharge process is evident from the differential capacities plot ($\Delta V = 0.001$ V) shown in Fig. 5b. Two oxidation/reduction peaks of LNM600 were found at 4.81/4.83 and 4.56/4.59 V, whereas those of LNM700 were found at 4.83/4.86 and 4.55/4.59 V. Similarly, two peaks in LNM800 were found at 4.80/4.87 and 4.55/4.60 V. According to Arrebola et al. [24], the main oxidation/reduction peaks in the range 4.5–5.0 V are associated with the $\text{Ni}^{2+}/\text{Ni}^{3+}$ and $\text{Ni}^{3+}/\text{Ni}^{4+}$ processes. The shapes of the two peaks are very important in terms of battery properties because the sharpness of such peaks at approximately 4.5–5.0 V is

related to the rate of lithium insertion and extraction [12]. This phenomenon could be associated with the improved crystallinity of the $\text{LiNi}_{0.5}\text{Mn}_{1.5}\text{O}_4$ cathode because of higher heat-treatment temperatures. At the 40th Li^+ insertion/extraction cycle, the variations of the charge/discharge behavior (Fig. 5c) and differential capacities (Fig. 5d) of LNM600, LNM700, and LNM800 were measured at 1 C. The discharge capacity (123.36 mAh/g) of LNM800 was much larger than those of LNM600 (81.17 mAh/g) and LNM700 (93.36 mAh/g). In addition, the main oxidation/reduction peak of LNM800 maintained sharp oxidation/reduction peaks compared to those of LNM600 and LNM700.

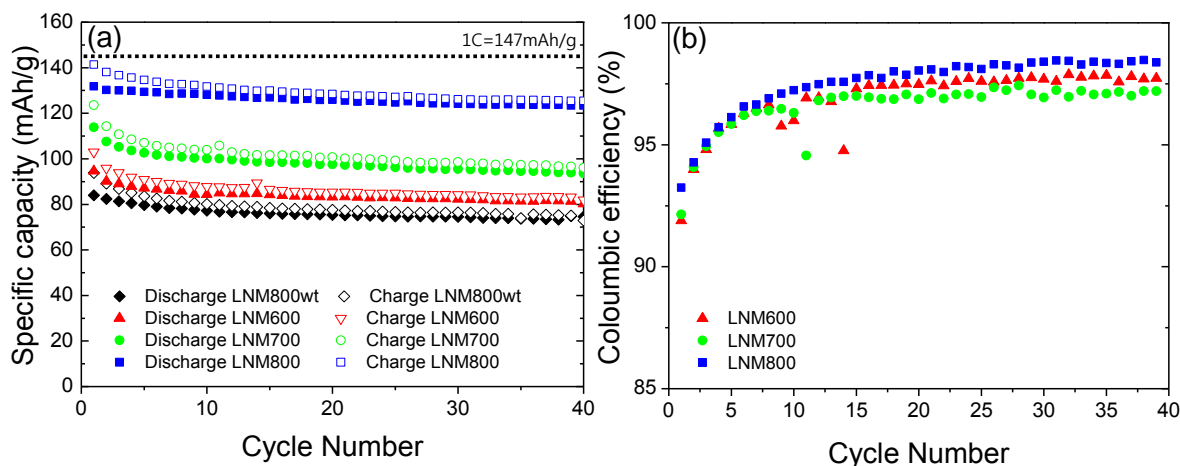


Figure 6. (a) Cycling performance and (b) Coulombic efficiencies of LNM600, LNM700, LNM800, and LNM800wt.

The discharge/charge capacities of $\text{LiNi}_{0.5}\text{Mn}_{1.5}\text{O}_4$ cathode materials with cycling were measured at the current density of 1 C; the results are displayed in Fig. 6a. The discharge/charge capacities of LNM600 at the 1st and 40th cycles were 94.60/102.96 and 80.24/81.95 mAh/g, respectively. For LNM700, the discharge/charge capacities (measured at 1 C) at the 1st and 40th cycles were 113.88/123.59 and 93.61/96.08 mAh/g, respectively, and the discharge/charge capacities (measured at 1 C) of LNM800 at the 1st and 40th cycles were 131.78/141.32 and 123.36/125.45 mAh/g, respectively. During the first five cycles, the capacities of both LNM600 and LNM700 significantly decreased compared to that of LNM800 because of the low stability. However, after the 5th cycle, all samples maintained good cycling stability over the charge/discharge process. As can be seen in Fig. 6b, the Coulombic efficiency of LNM800 approached 99% after 20 cycles. On comparing these three samples, we found that LNM800 showed a higher initial capacity and a better cycling stability than either LNM600 or LNM700 owing to its higher crystallinity and stability.

4. CONCLUSION

In this report, we used XRD and TG/DTA studies to elucidate the detailed reaction mechanism of single-crystal $\text{LiNi}_{0.5}\text{Mn}_{1.5}\text{O}_4$ -phase formation during a hydrothermal reaction followed by a heat

treatment. We also focused on the effect of heat-treatment temperatures on the electrochemical properties of $\text{LiNi}_{0.5}\text{Mn}_{1.5}\text{O}_4$ cathode materials. From a comparison of the final morphologies and electrochemical properties of the synthesized $\text{LiNi}_{0.5}\text{Mn}_{1.5}\text{O}_4$ materials with and without the prior hydrothermal reaction, we proved the effectiveness of the two-step synthesis process. The crystallinity was determined to play an important role in the improvement of the electrochemical properties in the $\text{LiNi}_{0.5}\text{Mn}_{1.5}\text{O}_4$ cathodes. Samples synthesized by the hydrothermal reaction followed by heat treatment at 800 °C showed an increased particle size and excellent cycling behaviors, which is probably owing to its higher crystallinity.

ACKNOWLEDGEMENTS

This research was financially supported by the Seoul Research and Business Development (R&BD) Program (WR090671) and by the Agency for Defense Development (ADD) of the Republic of Korea. Also, this work is supported by Korea Minister of Ministry of Land, Transport and Maritime Affairs (MLTM) as the U-City Master and Doctor Course Grant Program.

References

1. M. M. Thackeray, P. J. Johnson and L. A. de Picciotto, *Mater. Res. Bull.*, 19 (1984) 179.
2. M. M. Thackeray and A. De Kock, *J. Solid State Chem.*, 74 (1988) 414.
3. M. M. Thackeray, Y. Shao-Horn, A. J. Kahaian, K. D. Kepler, E. Skinner, J. T. Vaughey and S. A. Hacknet, *Electrochem. Solid State Lett.*, 1 (1998) 7.
4. M. M. Thackeray, *J. Electrochem. Soc.*, 142 (1995) 2558.
5. J. Cho and M. M. Thackeray, *J. Electrochem. Soc.*, 146 (1999) 3577.
6. X. Wang, H. Nakamura and M. Yoshio, *J. Power Sources.*, 110 (2002) 19.
7. K. Amine, H. Tukamoto, H. Yasuda and Y. Fujita, *J. Electrochem. Soc.*, 143 (1996) 1607.
8. Q. Zhing, A. Bonakdarpour, M. Zhang, Y. Gao and J. R. Dahn, *J. Electrochem. Soc.*, 144 (1997) 205.
9. T. Ohzuku, S. Takeda and M. Iwanaga, *J. Power Sources*, 81 (1999) 90.
10. R. Santhanam and B. Rambabu, *J. Power Sources*, 195 (2010) 5442.
11. R. Alcántara, M Jaraba, P Lavela and J.L Tirado, *Electrochim. Acta*, 47 (2002) 1829.
12. J. C. Arrebola, A. Caballero, M. Cruz, L. Hernán, J. Morales and E. R. Castellón, *Adv. Funct. Mater.*, 16 (2006) 1904.
13. J. H. Kim, S. T. Myung, C. S. Yoon, S. G. Kang and Y. K. Sun, *Chem. Mater.*, 16 (2004) 906.
14. K. M. Shaju and P. G. Bruce, *Dalton Trans.*, 40 (2008) 5471.
15. S. T. Myung, S. Komaba, N. Kumagai, H. Yashiro, H. T. Chung and T. H. Cho, *Electrochim. Acta*, 47 (2002) 2543.
16. X. Wu and S. B. Kim, *J. Power Sources*, 109 (2002) 53.
17. Y. S. Lee, Y.K. Sun, S. Ota, T. Miyashita and M. Yoshio, *Electrochem. Commun.*, 4 (2002) 989.
18. J. H. Kim, S. T. Myung and Y. K. Sun, *Electrochim. Acta*, 49 (2004) 219.
19. M. G. Lazarraga, L. Pascual, H. Gadjov, D. Kovacheva, K. Petrov, J. M. Amarilla, R. M. Rojas, M. A. Martin-Luengo and J. M. Rojo, *J. Mater. Chem.*, 14 (2004) 1640.
20. S. H. Park, S. W. Oh, S. T. Myung, Y. C. Kang and Y. K. Sun, *Solid State Ionics*, 176 (2005) 481.
21. X. Huang, Q. Zhang, J. Gan, H. Chang and Y. Yang, *J. Electrochem. Soc.*, 158 (2011) A139.
22. Y. J. Wei, L. Y. Yan, C. Z. Wang, X. G. Xu, F. Wu, and G. Chen, *J. Phys. Chem. B*, 108 (2004) 18547.
23. N. Deb, *J. Therm. Anal. Calorim.*, 81 (2005) 61.

24. Z. Zhao, J. Ma, H. Tian, L. Xie, J. Zhou, P. Wu, Y. Wang, J. Tao and X. Zhu, *J. Am. Ceram. Soc.*, 88 (2005) 3549.
25. K. M. Shaju and P. G. Bruce, *Dalton Trans.*, 40 (2008) 5471.

© 2013 by ESG (www.electrochemsci.org)